NASA/TM—1999-208902

AIAA–99–0638

In–Flight Aerodynamic Measurements of an Iced Horizontal Tailplane

Thomas P. Ratvasky
Lewis Research Center, Cleveland, Ohio

Judith Foss Van Zante
Dynacs Engineering Company, Inc., Brook Park, Ohio

Prepared for the
37th Aerospace Sciences Meeting and Exhibit
sponsored by the American Institute of Aeronautics
and Astronautics
Reno, Nevada, January 11–14, 1999

National Aeronautics and
Space Administration

Lewis Research Center

January 1999

Acknowledgments

The authors would like to thank the engineering and technical staff from the NASA Lewis Flight Operations and the Twin Otter crew. Special recognition goes to Mr. Richard Ranaudo for both his superb skills as a test pilot and his keen flight research insight, and to Dr. James Riley of the FAA for his contemplative oversight and diligent reviews. We thank John P. Dow, Sr., of the FAA Small Airplane Directorate, for his continued support and active promotion of the TIP.
We also would like to express our appreciation to the TIP sponsors:
NASA Aviation Operations Systems Base program
and the FAA Technical Center.

This report contains preliminary findings, subject to revision as analysis proceeds.

Available from

NASA Center for Aerospace Information
7121 Standard Drive
Hanover, MD 21076
Price Code: A03

National Technical Information Service
5285 Port Royal Road
Springfield, VA 22100
Price Code: A03

IN-FLIGHT AERODYNAMIC MEASUREMENTS OF AN ICED HORIZONTAL TAILPLANE

Thomas P. Ratvasky
Aerospace Engineer
NASA Lewis Research Center
Cleveland, OH 44135

Judith Foss Van Zante
Member, AIAA
Senior Engineer
Dynacs Engineering Co., Inc.
Brook Park, OH 44142

Abstract

The effects of tailplane icing on aircraft dynamics and tailplane aerodynamics were investigated using NASA's modified DHC-6 Twin Otter icing research aircraft. This flight program was a major element of the four-year NASA/FAA research program that also included icing wind tunnel testing, dry-air aerodynamic wind tunnel testing, and analytical code development. Flight tests were conducted to obtain aircraft dynamics and tailplane aerodynamics of the DHC-6 with four tailplane leading-edge configurations. These configurations included a clean (baseline) and three different artificial ice shapes. Quasi-steady and various dynamic flight maneuvers were performed over the full range of angles of attack and wing flap settings with each iced tailplane configuration. This paper presents results from the quasi-steady state flight conditions and describes the range of flow fields at the horizontal tailplane, the aeroperformance effect of various ice shapes on tailplane lift and elevator hinge moment, and suggests three paths that can lead toward ice-contaminated tailplane stall. It was found that wing flap deflection was the most significant factor in driving the tailplane angle of attack toward $\alpha_{tail\ stall}$. However, within a given flap setting, an increase in airspeed also drove the tailplane angle of attack toward $\alpha_{tail\ stall}$. Moreover, increasing engine thrust setting also pushed the tailplane to critical performance limits, which resulted in premature tailplane stall.

List of Symbols and Abbreviations

S&C	stability and control
C_l	section lift coefficient
C_{He}	elevator hinge-moment coefficient
C_T	thrust coefficient
G	acceleration due to gravity
cg	aircraft center of gravity
tail AOA	tailplane angle-of-attack, deg
tail beta	tailplane angle-of-sideslip, deg
TED	trailing edge down
TEU	trailing edge up

Greek:

$\alpha_{a/c}$,	aircraft angle-of-attack, deg
α_{tail}, α_t,	tailplane angle-of-attack, deg
$\beta_{a/c}$	aircraft angle-of-sideslip, deg
β_{tail}	tailplane angle-of-sideslip, deg
δE	elevator, aileron, and rudder, deg
δF, dF	flap deflection angle, deg

Introduction

Aircraft accident analyses have revealed ice contamination on horizontal tailplanes as the primary cause of over 16 accidents resulting in 139 fatalities. As a result, three International Tailplane Icing Workshops were convened by the FAA to appraise the collective experience on ice contaminated tailplane stall (ICTS) from aviation regulators, airframers, operators, and other interested parties. Recommendations from these meetings provided the motivation for NASA to develop the NASA/FAA Tailplane Icing Program (TIP)[1] to conduct research into the ICTS phenomenon.

The TIP was a four-year research program that utilized a combination of icing experts and test facilities that included NASA Lewis' Icing Research Tunnel (IRT), The Ohio State University (OSU) Low Speed Wind Tunnel, and NASA Lewis' DeHavilland DHC-6 Twin Otter Icing Research Aircraft.

One of the goals of this research was to improve the understanding of iced tailplane aeroperformance and aircraft dynamics. The objective of this paper is to provide the latest information on iced tailplane aeroperformance that was derived from quasi-steady

flight test data. The report is organized into sections that describe the role of the horizontal tailplane, the research aircraft, flight test procedures, results, and conclusions drawn from the work.

The Role of a Horizontal Tailplane

It has long been understood that airplanes require the horizontal tailplane to stabilize and control the aircraft in the pitch axis. For most conventional airplanes, the aircraft center of gravity (cg) is located forward of the wing aerodynamic center to provide acceptable stalling characteristics. The displacement of the wing lift from the cg causes a nose-down pitching moment. This moment is counteracted by an aerodynamic down load generated by the horizontal tail (see Figure 1).

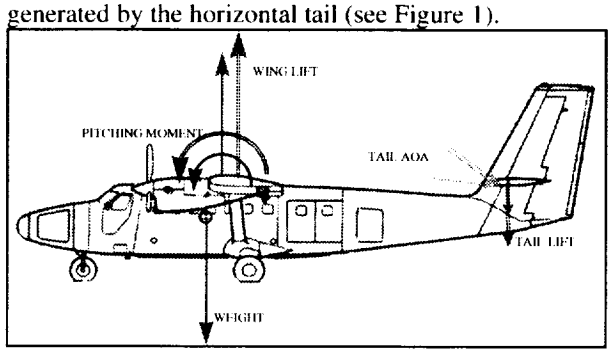

Figure 1 Force and Moment Diagram

Because the pitching-moment requirements vary throughout the flight envelope and aircraft configurations, the horizontal tailplane needs to be a variable lift-generating device. This is typically accomplished through deflection of the elevator and/or trim device (Figure 2).

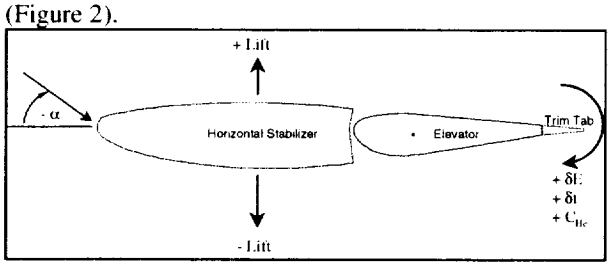

Figure 2 Typical Tailplane Component Diagram

Pitching-moment is strongly affected by flap deflection for several reasons. First, flap extension extends the chord-length of the wing and thereby increases the moment arm (h_n) of the wing lift. Secondly, wing lift will increase due to the increased camber of the wing. The combined result is an increased nose-down pitching moment that the horizontal tail must balance with an increased down load (see Figure 1 - double lines). Downstream of the flaps, the downwash assists the horizontal tail in performing its function by increasing the tail angle of attack (AOA). This increase in tail AOA may be too much or too little for the particular trim airspeed, in which case the elevator angle is adjusted by the pilot to either decrease or increase the tail down lift.

Wind tunnel results have shown that ice contamination on the tailplane causes several things to happen. The C_{lmax} and α_{stall} for a given elevator deflection are both reduced from the clean (baseline) case. Also, the hinge-moment can have a rapid shift at the iced α_{stall}. Results of this kind have been shown in several reports[2, 3, 4, 5] for a variety of tail geometries.

From accident and incident data, ICTS was typically experienced on the approach to landing phase, after flaps were extended and altitude was limited. Pilots reported "yoke-snatch" and sudden, uncommanded pitch down of the aircraft. The wind tunnel results listed above validate these reports. However, the data collected in this flight element of the TIP provides a greater insight into the complex nature of ICTS.

Research Aircraft

The NASA Icing Research Aircraft is a modified DHC-6 Twin Otter (Figure 3). It is powered by two 550-SHP Pratt and Whitney PT6A-20A turbine engines that drive three-bladed Hartzell constant-speed propellers. The primary flight controls are mechanically operated through a system of cables and pulleys. Control surfaces consist of elevator, ailerons, rudder, and wing flaps. Physical characteristics of the aircraft are in Table 1.

The aircraft was instrumented to acquire three distinct types of data: 1) aircraft dynamics 2) tail aeroperformance, and 3) video of tailplane flow visualization and pilot actions and visual cues. Each type of data and instrumentation is discussed below.

The aircraft dynamics data set included: inertial data, air data, control surface deflection data, pilot forces, engine parameters and airplane mass data.

Tail aeroperformance data consisted of tail inflow angles and velocities, as well as surface pressures. Three 5-hole probes were mounted to the leading edge of the left-side horizontal tail (Figure 4). Probe 1 was mounted near the tail tip, probe 2 was mounted mid-span, and probe 3 was mounted near the tail root. Each 5-hole probe measured the tailplane angle-of-attack (α_{tail}), tailplane angle-of-sideslip (β_{tail}), and dynamic pressure (q_{tail}) at the spanwise locations. The probes were extensively calibrated at NASA LeRC and OSU to determine α_{tail}, β_{tail} , and q_{tail} over the anticipated ranges encountered in flight.

Surface pressures around the horizontal tail were obtained using a pressure belt made from a series of strip-a-tube tygon tubing wrapped around the horizontal tail in a mid-span location (Figure 4). Each tube in the belt had a single hole cut at a specific chordwise location;

the end located on the tail was plugged. The other end was routed to a Scannivalve electronic scanning pressure transducer. In this way, the surface pressures about the tail were sensed at 50 holes on the pressure belt, and measured by the Scannivalve unit inside the aft section of the aircraft.

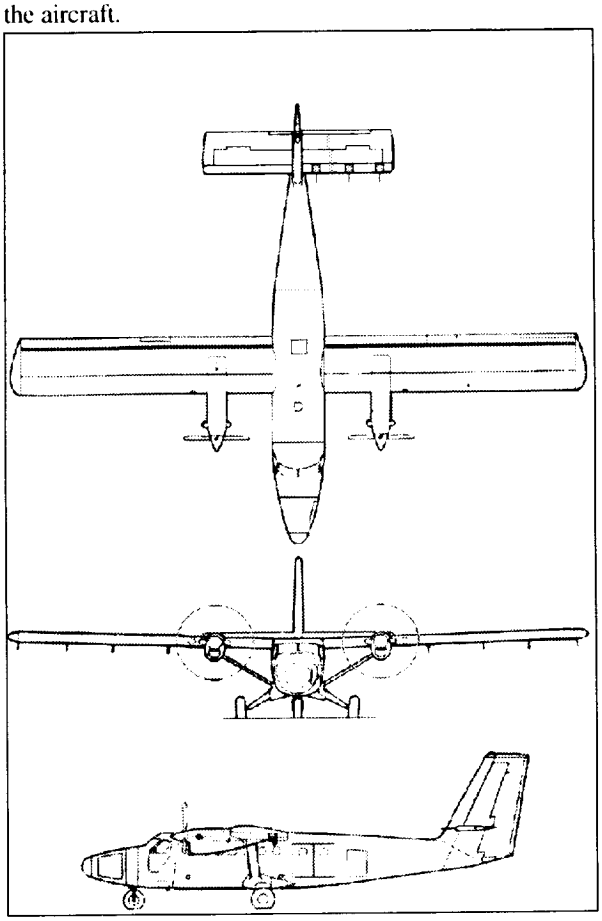

Figure 3 NASA Twin Otter Icing Research Aircraft

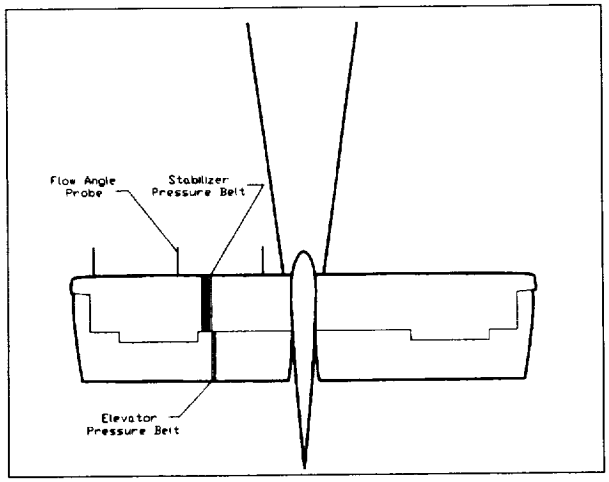

Figure 4 Tail Flow Probes and Pressure Belt

Flow visualization on the tailplane was accomplished by attaching yarn tufts to the lower surface of the horizontal tail and mounting a video camera to the bottom aft section of the fuselage. The tuft data provided real-time cues to the researchers when and where flow separation was occurring during the flight tests.

Another unique video system was installed to record the pilot actions during the maneuvers and also record the view through the windscreen to obtain the pilots perspective.

The total data set consisted of the three video signals and 95 data signals. The data signals were recorded at 100 Hz sampling frequency, and had 16-bit resolution. This data was recorded onto 8-mm tape using a ruggedized PC-compatible data acquisition system. The data on the 8-mm tapes was converted to ASCII files post-flight for further processing on ground-based computer systems.

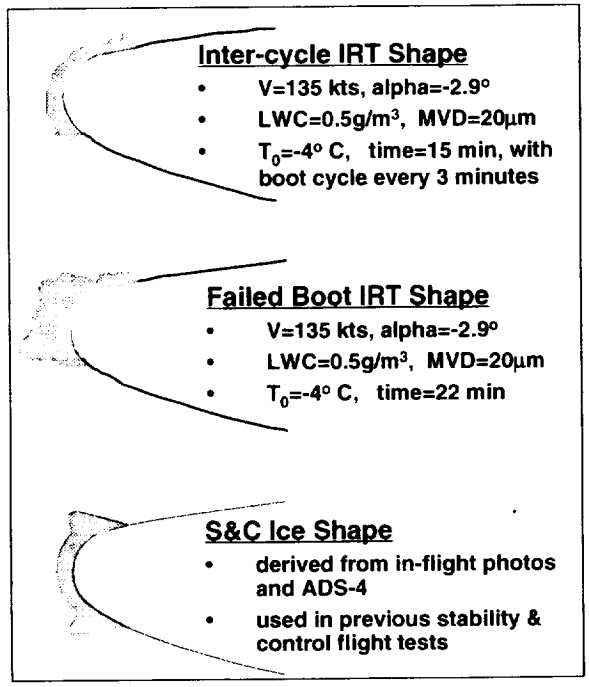

Figure 5 Schematic of ice shapes tested on the Twin Otter horizontal stabilizer

The Twin Otter was tested in a baseline configuration (clean tail), and with three simulated ice shapes (Figure 5). The first ice shape represented an inter-cycle residual ice accretion, the second represented a failed-boot ice accretion, and the third represented a generic glaze ice shape. The inter-cycle and failed boot shapes resulted from an IRT test on a Twin Otter tailplane model. These ice shapes were urethane casts made from molds of the ice that accreted during the IRT test, and

retained the rough 3D structure of the actual ice shape. The third shape was used extensively in NASA's previous stability and control tests, and was named the S&C ice shape. The S&C ice shape was cut from Styrofoam blocks, and did not incorporate 3D effects. These simulated ice shapes were attached to the leading edge of the horizontal stabilizers only. No other surfaces were contaminated.

Steady State Flight Test Procedures

Steady flight test points enabled a detailed examination of the effects of tailplane icing on aircraft forces & moments, tailplane lift and hinge moments, and elevator deflections required to trim the aircraft. The parameter space examined in this study varied the tailplane configuration [clean, inter-cycle ice, failed boot, S&C], the flap deflection (δF), the thrust setting (C_T), the aircraft airspeed (VTAS) & angle of attack ($\alpha_{a/c}$), and the aircraft sideslip angle ($\beta_{a/c}$). The full test matrix was conducted with a forward center of gravity (cg) location. In addition, a reduced number of test points were conducted with an aft cg. The following steady state profiles were used.

Steady-Wings-Level (SWL)

The aircraft was configured to a specific tail condition (clean/iced) and flap deflection angle (δF), and then the thrust setting (C_T) was fixed at the appropriate test speed. The aircraft was trimmed at an initial test speed, so that the elevator hinge moment was null. With the aircraft in a steady 1-G condition, data records were taken for approximately 15 seconds. Due to the fixed thrust setting, the aircraft was sometimes in a steady climb, level flight, or in a steady descent. After the initial test point, the next test speed was reached by adjusting the yoke position and resetting the throttles to obtain the consistent C_T. The elevator would not be retrimmed, so that the yoke force required to hold the elevator in that position could be translated into an elevator hinge moment (C_{He}). This procedure was repeated for four to six airspeeds at each thrust setting, flap deflection and tail ice configuration. All of these test points were done with minimal sideslip ($\beta \approx 0$) on the aircraft.

Steady-Heading Sideslips (SHSS)

A limited number of steady-heading sideslips (SHSS) test points were obtained. The procedure was similar to the steady-wing-level points, except that the aircraft was put into approximately a 17° sideslip to the right and to the left, while maintaining a specified airspeed, flap angle and thrust coefficient. The sideslip was accomplished by the pilot applying either right or left rudder and cross-controlling with left or right aileron to yaw and roll the aircraft into a steady-heading sideslip.

Results

Tailplane Flow Field

The flow field at the tailplane is very complex due to aircraft features like wings, flaps, fuselage, and propulsion systems, which may be upstream of the tail. Each feature has various amounts of influence on the flow field and, consequently, affects the tailplane performance. Data from the tail flow probes provided insight into the range of flow fields in which the tailplane was required to function. Figure 6 shows the tail AOA versus airspeed for flap deflections from 0 to 40 degrees.

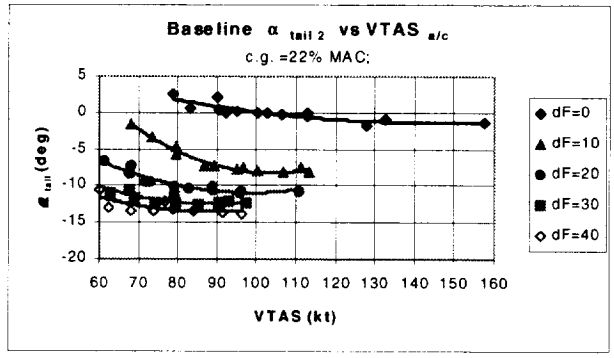

Figure 6 Tail AOA vs Aircraft Airspeed

From these plots, the relationship between tail AOA and aircraft airspeed is apparent. The tail AOA clearly became more negative as the aircraft speed increased for a given flap deflection. The relationship could be characterized by a 2nd order polynomial and illustrates the change in tail AOA due to a decrease in both $\alpha_{a/c}$ and wing downwash as the aircraft airspeed was increased. Downwash decreased with increased airspeed because the lift coefficient was reduced. Within a given flap setting, the typical change in tailplane AOA ($\Delta\alpha_t$) due to increased airspeed was $\Delta\alpha_t$= -4°. However, with δF=10°, the $\Delta\alpha_t$= -7°.

More importantly, flap deflection caused significant negative bias shifts in the tailplane AOA. Initial flap deflection from 0-10 degrees had the most significant effect on tailplane AOA, causing $\Delta\alpha_t \approx$ -7°. As flaps were further deflected, the negative shift in α_{tail} decreased such that when flaps were deflected from 30-40 degrees, $\Delta\alpha_t$= -1°. Overall, as the flaps were fully deflected from δF=0-40° at a constant airspeed of 90 knots, the $\Delta\alpha_t$= -14°. The shifts in α_{tail} when flaps were deflected were due to the increase in wing downwash and decrease in aircraft AOA.

In addition to the angle of attack variations, there were variations in spanwise flow at the horizontal tail even with the aircraft at $\beta_{a/c}=0°$. **Figure 7** shows the tail sideslip angle (β_{tail}) measured at mid-span flow probe for various airspeeds and flap angles.

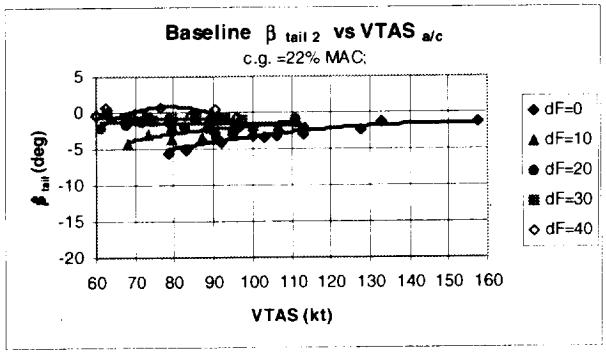

Figure 7 Tail Sideslip vs Aircraft Airspeed

For flaps settings, $\delta F=[0°, 10°]$, there was a pronounced inboard flow increase at the slower airspeeds. This was considered to be an effect of the propeller slipstream. As flaps increased beyond 10°, this effect was minimal because the slipstream passed below the horizontal tail.

Steady heading sideslip (SHSS) test points revealed more on the complex flow field presented to the horizontal tailplane. Figure 8 shows the effects of aircraft sideslip on tailplane sideslip measured by the mid-span flow probe. Note that these data are for an aft cg. There was nearly a one-to-one relationship between aircraft sideslip and tailplane sideslip with a small positive bias shift in tail beta. The effect of flap deflection was minimal. However, the effect of SHSS on tail AOA was of greater consequence (Figure 9). As the airplane was placed in a positive sideslip, the tail AOA became more positive. Negative sideslip angles seemed to have minimal effect on the tail AOA.

A possible reason for this behavior is the position of the probe with respect to the fuselage. When the aircraft was in a positive sideslip, the fuselage was upwind of the flow probe, which may have altered the flow direction at the tailplane. When the aircraft was in negative sideslip, the fuselage was not in a position to have a significant effect on the mid-span flow probe. However, it is reasonable to assume the right side of the tailplane was undergoing the exact opposite situation, where a more positive tail AOA existed during a negative sideslip. Flow visualization using yarn tufts support these results because flow separation caused by the ice shapes on the tail was alleviated when the aircraft was placed into a sideslip in either direction.

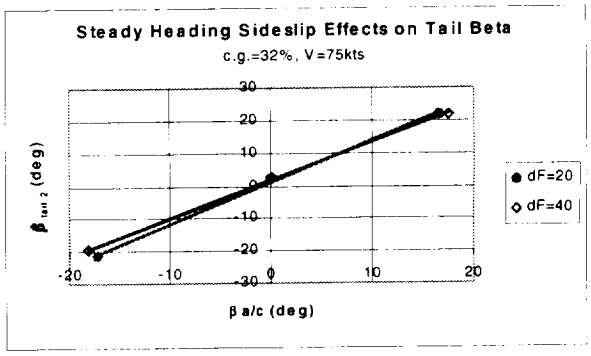

Figure 8 SHSS Effects on Tail Beta

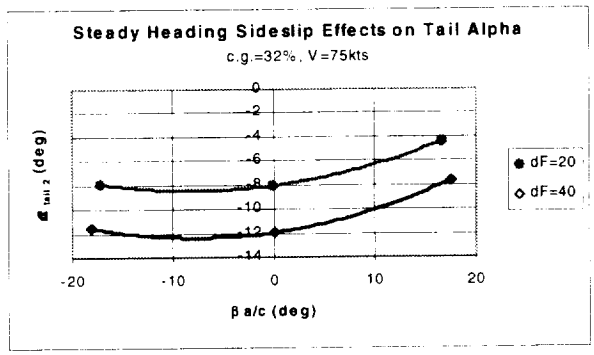

Figure 9 SHSS Effects on Tail AOA

Another contributor to the flow field at the tail is the propeller thrust. Figure 10 shows the relationship between thrust coefficient, C_T and tail AOA. As thrust was increased and velocity held constant, the tail AOA decreased for all flap settings. The thrust influence was greatest with $\delta F=10°$, where $\Delta\alpha_t= -7°$ as thrust increased from $C_T=0$ to 0.10. For the other flap settings, the typical $\Delta\alpha_t= -3°$ over the ranges of thrust tested from idle to a normal cruise power. The trends indicate that thrust coefficients higher than those tested would yield an even greater decrease in tail AOA.

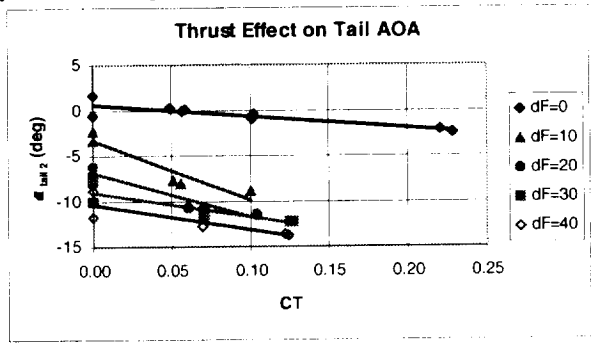

Figure 10 Thrust Effect on Tail AOA

Tailplane Aeroperformance

As discussed in an earlier section, the role of the horizontal tailplane is to provide stability and control in the pitch axis, and to do so for the full range of flow fields presented to it. As seen in the previous section, there can be a wide range of flow fields presented to the tailplane, and to maintain acceptable stability and controllability, the horizontal tailplane must have the capability to vary the load generation. This is achieved by moving either the elevator or trim setting.

Ice on the horizontal tail did not significantly modify the flow field coming into the tailplane. However, ice did affect the tail lift, drag, pitching and hinge moment characteristics. But since in flight the tail down load requirements are the same regardless of the ice contamination (for a given cg, a/c configuration, and flight condition), the effect of ice was not easily observed in the integrated tail lift coefficient. Figure 11-Figure 13 display the tail section lift coefficient required for holding the steady airspeed for each tail configuration. Clearly, the tail lift coefficient required is nearly the same within each flap setting and all ice shapes.

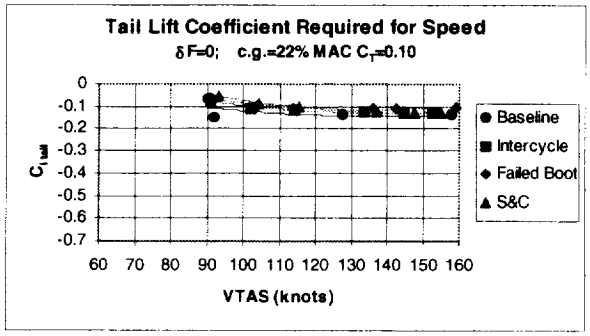

Figure 11 Ice Effects on Tail C_l, δF=0°

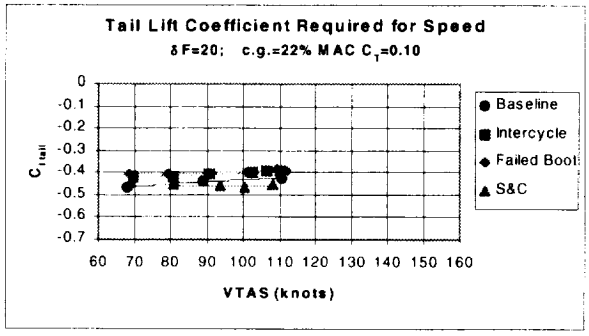

Figure 12 Ice Effects on Tail C_l, δF =20°

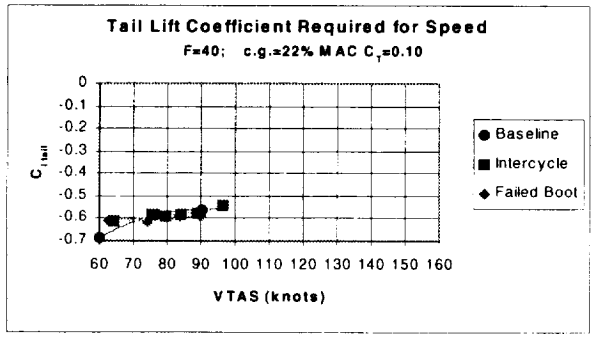

Figure 13 Ice Effects on Tail C_l, δF =40°

With ice on the tail, the required tail down load was achieved through greater elevator deflection as seen in Figure 14-Figure 16. For flaps at 0 degrees (Figure 14), all speed points required the same amount of elevator deflection for each tail configuration. This implies that the effect of the ice was negligible at the range of tailplane AOA's observed with flaps at 0 degrees.

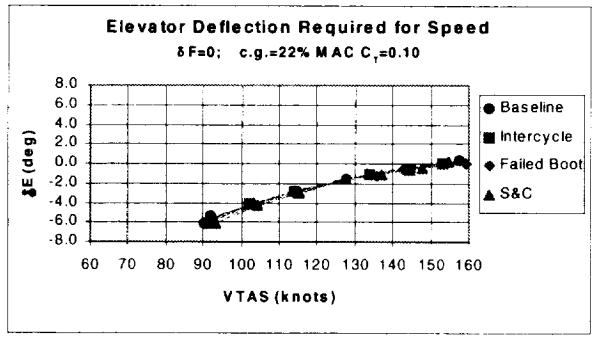

Figure 14 Ice Effects on δE, δF=0°

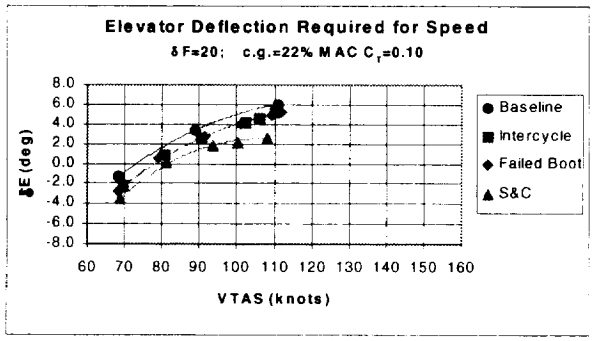

Figure 15 Ice Effects on δE, δF=20°

As the flaps were deflected to 20 degrees, the tailplane AOA increased and the relative aerodynamic degradation between the ice shapes became apparent. The greatest change in elevator deflection (ΔδE) was observed with the S&C ice configuration. The S&C ice reduced tail lift such that the elevator needed to be deflected 3-4° more than the baseline to obtain the tail

lift required to maintain trim speed. The inter-cycle and failed boot ice also required more TEU elevator deflection from the baseline, but only about 1° more for δF=20° case.

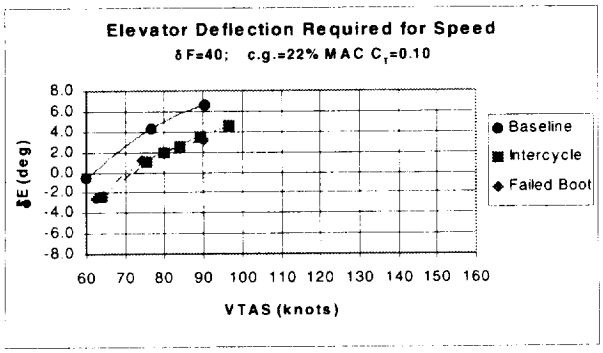

Figure 16 Ice Effects on δE, δF=40°

With flaps deflected to δF=40°, the S&C ice was not tested due to safety of flight, but the inter-cycle and failed boot ice both showed an equal decrease in aeroperformance capability by requiring a Δδ E=3-4° TEU shift from the baseline to maintain trim airspeed. The similarity between the inter-cycle and the failed boot ice is understood after examining the wind tunnel results of Gregorek, et al [Ref 5]. For the tailplane AOA and δE range observed at the δF=40° case, the C_l for both ice cases happened to be the same as indicated in Ref 5. Therefore, the change in elevator deflection, Δδ E, required to make up the ΔC_l was likewise similar.

Clearly, the change in elevator deflection required to maintain speed is a good indicator of the loss of tailplane capability. In addition to this indicator, the hinge moment data provides greater insight into the severity of the degradation and provides a direct connection to the piloting task of flying with an ice-contaminated tailplane.

Figure 17-Figure 19 show the effect of ice on the elevator hinge moment as a function of speed for three flap settings. Recall that the test points were initiated from a trimmed slow speed, with each successive test point obtained by the pilot moving the yoke forward to increase the airspeed. The pilot force was translated into a hinge moment using gearing ratio and tail geometry values.

With flaps at δF=0° (Figure 17), there were negligible differences in hinge moment between the clean and various iced configurations. These results are consistent with the low tail AOA, low tail C_l, and δE results.

However, with the flaps deflected to δF=20° (Figure 18), a clear breakout from the baseline was most notable for the S&C ice contamination. As the airspeed increased from 80 knots, control force lightening occurred. At the 108 knot test point, the control forces were neutral and heading towards a control force reversal. The hinge moment data for the inter-cycle and failed boot ice configurations differed little from the baseline.

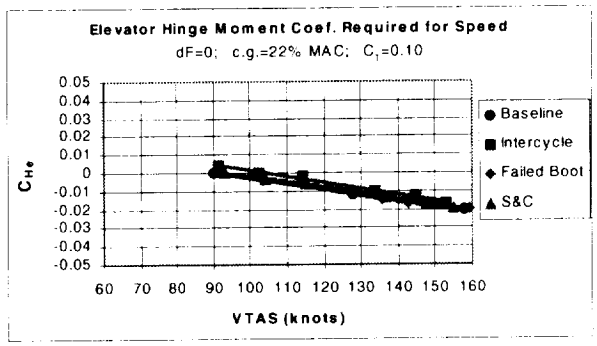

Figure 17 Ice Effects on C_{He}, δF=0°

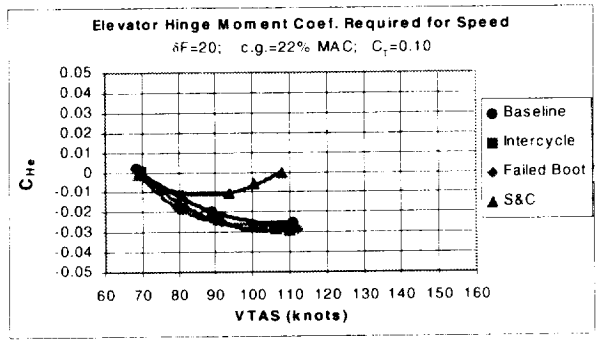

Figure 18 Ice Effects on C_{He}, δF=20°

As the flaps were extended to δF=40° (Figure 19), the S&C ice shape was not tested due to safety of flight, but a strong breakout between the inter-cycle and failed boot from the baseline hinge-moment was observed.

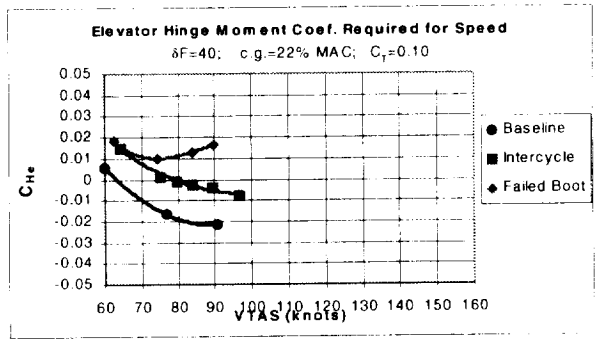

Figure 19 Icing Effects on C_{He}, δF=40°

One point to note first was that the elevator forces were not trimmable for any of the tail configurations, i.e. all were initiated from a pull-force by the pilot to obtain the initial speed point. Another point to note was the difference in the initial hinge moment required

between the baseline and iced cases. In the previous examples, all cases began at the same (C_{He}=0) trim point. The $\Delta C_{He} \approx 0.015$ relates to a 7-pound pull force for this aircraft and airspeed. As the airspeed increased, the baseline required a push force (negative C_{He}) as is normal.

For the Inter-cycle ice, the pull force was reduced as the airspeed was increased to 80 knots and then a push force was used to further increase airspeed. This case does not demonstrate control force reversal or lightening since the progressive points do not exceed the initial or preceding test points. This case would be similar to operating with a trim tab setting for 80 knots and pulling back on the yoke to achieve the 62 knot test point.

The hinge moment for the failed boot ice configuration was initially reduced as airspeed increased, but then required an increased pull force to achieve the speed points above 75 knots. This case does demonstrate a control force reversal since the progressive speed points required pull-forces greater than the initial force and demonstrated the yoke-snatch scenario.

Another interesting point that is observed in Figure 19, was the reduced effectiveness of the trim tab. In the iced cases, the trim tab was fully deflected for nose-up command [trim tab TED, elevator TEU] (see Figure 20). The inter-cycle ice reduced the effectiveness of the trim tab to provide only enough authority to counterbalance the elevator angle for an 80 knot speed point. With the failed boot ice, the forces were untrimmable for any speed point, which resulted from a trim tab rendered ineffective by the flow separation behind the ice contamination.

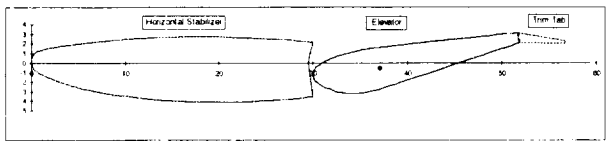

Figure 20 Horizontal Tailplane Components

Paths to Stall

Results from the flow field and aeroperformance analyses provide evidence of three paths that can lead to tailplane stall due to ice contamination by providing a highly negative tailplane AOA. These paths are:

- Increasing flap deflection
- Increasing airspeed
- Increasing thrust *(may be airplane and/or configuration specific)*

As was reviewed in previous sections, the flap deflection had the largest affect on tailplane AOA, but within each flap deflection case, an increase in airspeed and an increase in thrust further increase the negative tailplane AOA. Depending on the severity of ice contamination, these combinations of aircraft configurations and flight conditions led to control force lightening, control force reversal, or full tailplane stall.

Conclusions

Flight tests were conducted on a twin-engine turbopropeller airplane to expand the understanding of horizontal tailplane aeroperformance with and without ice contamination. The flow field at the tailplane was measured in order to gain an understanding of the range of flow angles that the tailplane must operate in. Flow fields at the tail were most affected by wing flap deflection, but were also influenced by aircraft angle of attack and sideslip, and propeller thrust.

Tailplane section lift was measured with a no-ice baseline and various levels of ice contamination on the leading edge for a full range of flap deflections and airspeeds. The ice contamination had only minor changes in the integrated tailplane section lift. The primary reason for this result was the tail down load requirement for each case was the same regardless of contamination level.

Ice contaminated tail down loads were achieved by increasing the camber of the tailplane through additional elevator deflection. The change in elevator deflection angle required for trim became a good indicator of the degradation of tailplane performance.

Additionally, it was shown that elevator hinge moment provided a greater resolution to the degradation caused by the various ice shapes and clearly indicated control force lightening and reversal for some aircraft and ice configurations and flight conditions.

The results from this steady-state analysis of an ice-contaminated tailplane are an important addition to the work already completed by others in the industry. However, it is recognized that these comprehensive data sets and results are limited to one airplane configuration, and that the ICTS phenomenon may have many configuration specific subtleties.

Acknowledgments

The authors would like to thank the engineering and technical staff from the NASA Lewis Flight Operations and the Twin Otter crew. Special recognition goes to Mr. Richard Ranaudo for both his superb skills as a test pilot and his keen flight research insight, and to Dr. James Riley of the FAA for his contemplative oversight and diligent reviews. We thank John P. Dow, Sr., of the FAA Small Airplane Directorate, for his continued support and active promotion of the TIP. We also would like to express our appreciation to the TIP sponsors: NASA Aviation Operations Systems Base program and the FAA Technical Center.

Table 1: Aircraft Geometric Properties

Characteristic	Low	High
Mass, kg	4,510	4,970
Inertia		
IX, kg-m^2	26,190	26,660
IY, kg-m^2	33,460	34,650
IZ kg-m^2	47,920	51,650
IXZ, kg-m^2	1,490	1,560
Wing Geometry:		
Area, m^2	39.02	
Aspect Ratio	10.06	
Span, m	19.81	
Mean geometric chord, m	1.98	
Airfoil Section	"DeHavilland High Lift" 17% thickness	
Horizontal Tail:		
Area, m^2	9.14	
Aspect ratio	4.35	
Span, m	6.30	
Mean geometric chord, m	1.45	
Airfoil Section (inverted)	NACA 63_A213	
Tail Volume	0.94	

References

1 Ratvasky, T. P., "NASA/FAA Tailplane Icing Program Work Plan," April 1994

2 Ingelman-Sundberg, M., Trunov, O.K., "Wind Tunnel Investigation Of The Hazardous Tail Stall Due To Icing," Swedish-Soviet Working Group on Flight Safety Report No. JR-2. 1979

3 Trunov, O.K., Ingelman-Sundberg, M., "On The Problem Of Horizontal Tail Stall Due To Ice," Swedish-Soviet Working Group on Flight Safety Report No. JR-3. 1985

4 Hiltner, D.W., McKee, M., La Noé, K.B., "DHC-6 Twin Otter Tailplane Airfoil Section Testing in The Ohio State University 7x10 Wind Tunnel," 1995, being reviewed for publication

5 Gregorek, G.M., Dreese, J.J., La Noé, K.B., "Additional Testing of the DHC-6 Twin Otter Iced Airfoil Section at The Ohio State University 7'x10' Wind Tunnel," 1996, being reviewed for publication

REPORT DOCUMENTATION PAGE

Form Approved
OMB No. 0704-0188

1. AGENCY USE ONLY (*Leave blank*)	2. REPORT DATE	3. REPORT TYPE AND DATES COVERED
	January 1999	Technical Memorandum

4. TITLE AND SUBTITLE

In–Flight Aerodynamic Measurements of an Iced Horizontal Tailplane

5. FUNDING NUMBERS

WU–548–21–23–00

6. AUTHOR(S)

Thomas P. Ratvasky and Judith Foss Van Zante

7. PERFORMING ORGANIZATION NAME(S) AND ADDRESS(ES)

National Aeronautics and Space Administration
Lewis Research Center
Cleveland, Ohio 44135–3191

8. PERFORMING ORGANIZATION REPORT NUMBER

E–11503

9. SPONSORING/MONITORING AGENCY NAME(S) AND ADDRESS(ES)

National Aeronautics and Space Administration
Washington, DC 20546–0001

10. SPONSORING/MONITORING AGENCY REPORT NUMBER

NASA TM—1999-208902
AIAA–99–0638

11. SUPPLEMENTARY NOTES

Prepared for the 37th Aerospace Sciences Meeting & Exhibit sponsored by the American Institute of Aeronautics and Astronautics, Reno, Nevada, January 11–14, 1999. Thomas P. Ratvasky, NASA Lewis Research Center and Judith Foss Van Zante, Dynacs Engineering Company, Inc., 2001 Aerospace Parkway, Brook Park, Ohio 44142 (work funded under NASA Contract NAS3-98008). Responsible person, Thomas P. Ratvasky, organization code 5840, (216) 433–3905.

12a. DISTRIBUTION/AVAILABILITY STATEMENT

Unclassified - Unlimited
Subject Categories: 08, 03 and 05 Distribution: Nonstandard

This publication is available from the NASA Center for AeroSpace Information, (301) 621–0390.

12b. DISTRIBUTION CODE

13. ABSTRACT ***(Maximum 200 words)***

The effects of tailplane icing on aircraft dynamics and tailplane aerodynamics were investigated using NASA's modified DHC-6 Twin Otter icing research aircraft. This flight program was a major element of the four-year NASA/FAA research program that also included icing wind tunnel testing, dry-air aerodynamic wind tunnel testing, and analytical code development. Flight tests were conducted to obtain aircraft dynamics and tailplane aerodynamics of the DHC-6 with four tailplane leading-edge configurations. These configurations included a clean (baseline) and three different artificial ice shapes. Quasi-steady and various dynamic flight maneuvers were performed over the full range of angles of attack and wing flap settings with each iced tailplane configuration. This paper presents results from the quasi-steady state flight conditions and describes the range of flow fields at the horizontal tailplane, the aeroperformance effect of various ice shapes on tailplane lift and elevator hinge moment, and suggests three paths that can lead toward ice-contaminated tailplane stall. It was found that wing flap deflection was the most significant factor in driving the tailplane angle of attack toward $\alpha_{\text{tail stall}}$. However, within a given flap setting, an increase in airspeed also drove the tailplane angle of attack toward $\alpha_{\text{tail stall}}$. Moreover, increasing engine thrust setting also pushed the tailplane to critical performance limits, which resulted in premature tailplane stall.

14. SUBJECT TERMS	15. NUMBER OF PAGES
Aircraft icing; Stability and control; Tailpipe icing; Tailplane performance	15
	16. PRICE CODE: A03

17. SECURITY CLASSIFICATION OF REPORT	18. SECURITY CLASSIFICATION OF THIS PAGE	19. SECURITY CLASSIFICATION OF ABSTRACT	20. LIMITATION OF ABSTRACT
Unclassified	Unclassified	Unclassified	